



Multi-channel AgNWs-doped interdigitated organic electrochemical transistors enable sputum-based device towards noninvasive and portable diagnosis of lung cancer



Ru Zhang^{a,1}, Jing Zhang^{b,1}, Fei Tan^{c,d}, Deqi Yang^a, Bingfang Wang^a, Jing Dai^a, Yin Qi^b, Linyu Ran^b, Wenjuan He^b, Yingying Lv^e, Feilong Wang^{b,**}, Yin Fang^{a,*}

^a Research Center for Translational Medicine, Key Laboratory of Arrhythmias of the Ministry of Education of China, Shanghai East Hospital; The Institute for Biomedical Engineering & Nano Science, Tongji University School of Medicine, Shanghai, 200120, China

^b Department of Pulmonary and Critical Care Medicine, Shanghai East Hospital, Tongji University, Shanghai, 200120, China

^c Department of ORL-HNS, Shanghai Fourth People's Hospital, And School of Medicine, Tongji University, Shanghai, China

^d The Royal College of Surgeons of England, London, UK

^e Research Centre of Nanoscience and Nanotechnology, College of Science, Shanghai University, Shanghai, 200444, China

ARTICLE INFO

Keywords:

AgNWs-doped
Multi-channel
Organic electrochemical transistors
Biosensor
Noninvasive
Sputum

ABSTRACT

Biochemical monitoring of bodily fluids such as sweat, urine, and tears have been extensively developed, but reliable biochemical analysis of sputum biospecimens remains limited and challenging due to the low abundance of biomarkers in intrinsically viscous sputum. We reported a portable multi-channel sputum-based interdigitated organic electrochemical transistors (SiOECTs) device for noninvasive sputum diagnosis. We tailored the AgNWs-doped organic electrochemical transistors, integrating with multiplexed aptamer-antigen assays, to realize the signal amplification and simultaneous detection of biomarkers in raw sputum biospecimens from lung cancer patients. Clinical validation studies demonstrated favorable correlation coefficients between the sputum and serum biospecimens. By utilizing our portable multi-channel iOECTs devices, lung cancer patients were differentiated from health control with an optimum area under the curve (AUC) of 0.931, sensitivity of 87.0%, and specificity of 86.5%. Our miniaturized and portable device could even realize the continuous in-home tracking of the biomarkers change for lung cancer patients after radiotherapy/chemotherapy. It is envisaged that the SiOECTs will shed light on noninvasive diagnostics platforms for sputum-related diseases.

1. Introduction

Biochemical monitoring of physiological phenomena via bodily fluids like saliva, sweat, urine, and tears offers new insights and opportunities to ameliorate diagnostics efficiency radically [1,2]. Portable bioelectronic devices have been applied to point-of-care diagnostics with virtues of convenient operation, noninvasiveness, and inherent miniaturization [1,3,4]. Although sweat/tears-based portable bioelectronics has been well developed thus far, biomarkers extracted from deep tissues are hardly accessible [5,6]. Sputum-based portable bioelectronics is an attractive candidate for noninvasive diagnosis and monitoring, and the patients can achieve real-time diagnosis and in-home monitoring without the restriction of instruments [7,8]. Moreover, sputum would be

obtained via a noninvasive sampling strategy, which is preferable for most patients [9–11]. Specifically, the human sputum is a secretion from the lung, trachea, and bronchi. A high correlation between sputum and lung-related diseases in the respiratory system has been demonstrated [12–14]. However, the increase of acid glycoprotein in sputum and subsequent cross-linking of glycoprotein via disulfide bond and hydrogen bond leads to high viscosity and elasticity of sputum specimen. It poses two foreseeable challenges of low abundance biomarkers and necessary pretreatment in the accurate sputum biospecimens diagnosis [15,16].

Organic electrochemical transistors (OECTs) biosensors have attracted intensive attentions for various quantified diagnostics applications due to the merits of intrinsic amplification effect, high signal-noise ratio, and accessible integration with multiplexed bioelectronics [17–21].

* Corresponding author.

** Corresponding author.

E-mail addresses: wang_feilong@tongji.edu.cn (F. Wang), yin_fang@tongji.edu.cn (Y. Fang).

¹ Equal contributing authors.

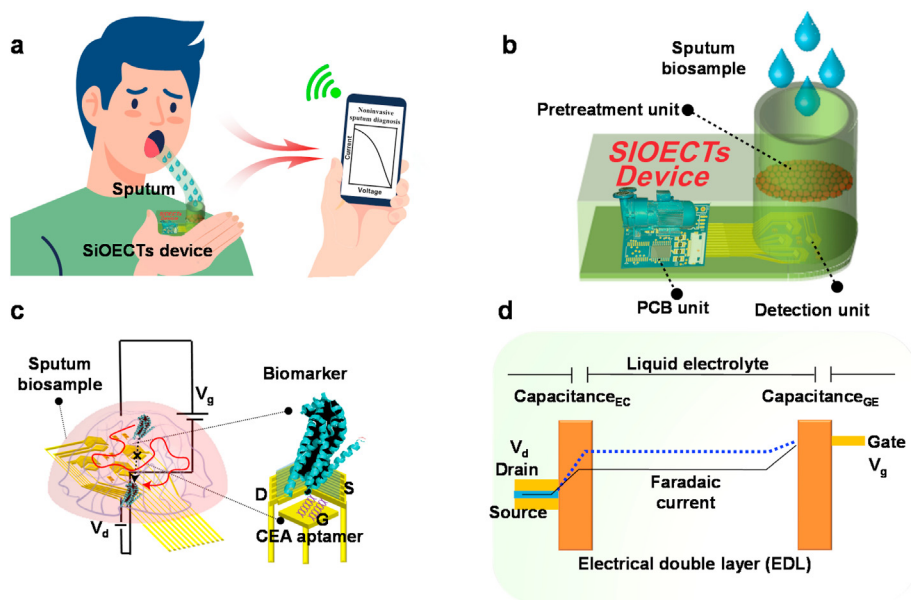


Fig. 1. Design and biosensing mechanism of SiOECTs platform. a) Detection scenario of SiOECTs when a lung cancer patient expectorates sputum into a portable SiOECTs device. b) Enlarged photograph of SiOECTs, demonstrating its hierarchical architecture. c) Detection mechanism of SiOECTs via AgNWs-doped interdigitated organic electrochemical transistors biosensor and d) corresponding equivalent circuit and electrical double layer effect. Capacitance_{GE} between the gate and the electrolyte and the capacitance_{EC} between channel and the electrolyte constitute the EDL.

Notably, the semiconductor doping effect is a critical factor for the amplification of OECTs [22,23]. Electrically conductive materials, such as silver nanowires (AgNWs) have been thought to be electron mediators that enhance the electronic mobility/volumetric charge storage capacity and thus assist the ion-electron transfer process [24]. Moreover, excellent OECTs rely on acceptable electronic transport and effective ion penetration from the electrolyte into the semiconductor channel, which are inextricable prerequisites for amplifying small biochemical signals into appreciable readouts. Sputum with viscous bio gels hinders the ion-electron transfer process, which limits the design of advanced OECTs-based sputum-analytical platform. Therefore, reducing the heterogeneity and high viscosity of sputum biospecimen to recover the ionic-electron transport is of great significance for developing noninvasive sputum-based OECTs diagnostic bioelectronic devices, although its research in this area is almost vacant.

Herein, we developed sputum-analytical biosensors by enhancing the mobility and ultrasensitivity (down to ~pg/mL) of the OECTs device. We introduced the AgNWs-doped organic electrochemical transistors biosensors to recover the ion/electron transport process in the sputum. The multiplexed, ultrasensitive biosensors were then assembled into a miniaturized, wrist-portable device to realize the sputum-based real-time diagnosis and in-home monitoring. Lung cancer, which is closely related to sputum [12,13], was chosen as a model to verify the functionality and versatility of our sputum-based diagnosis device. The AgNWs-doped organic electrochemical transistor arrays with interdigitated-electrode architecture simultaneously enhanced the quantifications of panel biomarkers of CEA, NSE, and CA125 with good selectivity and reliability. Notably, the wrist-portable SiOECTs devices were evaluated against clinic-used assay and demonstrated presentable linearity and high correlation coefficient (CEA: $R^2 = 0.963$) even via noninvasive sputum specimen testing. Furthermore, the SiOECTs based point-of-care testing (POCT) device has been successfully applied to the multiplexed diagnosis of lung cancer patients as a comparison against healthy individuals with the enhanced area under the curve (AUC) of 0.931, sensitivity of 87.0%, and specificity of 86.5%. Due to the merits of quick response, high signal-noise ratio, miniaturization, and wrist-portability, our device enabled continuous in-home tracking for the biomarker changes of lung cancer patients after radiotherapy/chemotherapy.

2. Results and discussions

2.1. Materials, design, integration of SiOECTs and its sensing strategies

The detection scenario of our SiOECTs for noninvasive sputum diagnosis towards lung cancer surveillances was schematically illustrated in Fig. 1a when a patient expectorates sputum into the device. The portable SiOECTs device (Fig. 1b) introduced here involved the pretreatment unit, multi-target organic electrochemical transistors biosensors, and the electronic system for pretreatment, collection, and biochemical analysis of sputum specimen. The pretreatment unit, including sputum reservoir encapsulation, was fabricated via 3D printing of polylactic acid (PLA) with tailored architecture. The architectural layout of the SiOECTs device was illustrated in Fig. S1a with dimensional details in Fig. S1b-c. The device was integrated with a microcontroller unit (MCU) and built-in digital to analog converters (DACs, Fig. S2, Supporting Information). When a patient initiates a detection, the equipped DAC will launch a drain-source and gate voltage, relying on amperometric measurement via a SiOECTs device. To record multiplexed amperometric currents of SiOECTs for quantifying biomarkers, the analog to digital converters (ADCs) would track the resultant currents flowing through corresponding electrodes. Subsequently, the recorded data were transmitted to the storage center via a WiFi module for continuous monitoring (Fig. S2, Supporting Information). The multi-channel biosensor was laminated on a polyethylene terephthalate (PET, thickness of 0.188*mm, Grafix DURA-RAR) substrate with hierarchical architecture including metal interconnection (Cr/Au), AgNWs@PEDOT:PSS layer, and a SU-8 passivation layer (Fig. S3a-b, Fig. S3 Supporting Information). For the biochemical diagnosis of sputum-related disease (e.g., lung cancer), the SiOECTs device was functionalized with aptamers for specific binding of CEA, NSE, and CA125, respectively (Fig. 1c, Fig. S3b, and S4, Supporting Information). Capacitance_{GE} between the gate and the electrolyte and the capacitance_{EC} between the channel and the electrolyte constitute the electric double layer (EDL). When the biochemical reaction occurs, the small signal on the aptamer-functionalized gate will be amplified to the channel current through the electrical double layer effect, thus realizing sensitive detection [25–27]. The biosensing mechanism of SiOECTs could be illustrated by

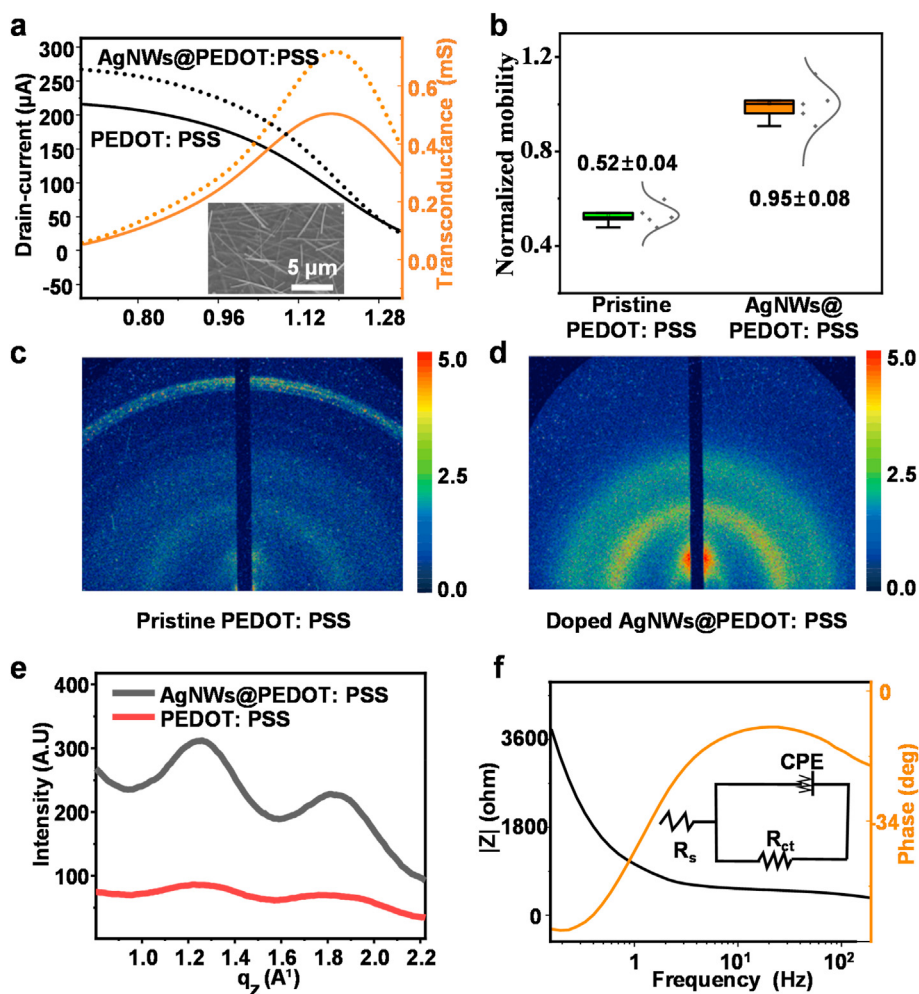


Fig. 2. Characterizations and validations of AgNWs-doped process towards SiOECTs devices. a) The comparisons of transfer characteristics and corresponding transconductance for pristine PEDOT: PSS and doped AgNWs@PEDOT: PSS. The inset is the SEM photography of AgNWs@PEDOT: PSS. b) Statistical analysis of normalized mobility due to the doping of AgNWs. The normalized mobility of AgNWs@PEDOT: PSS was enhanced from 0.52 ± 0.04 to 0.95 ± 0.08 ($n = 5$) due to the doping. 2D GISAXS image of c) pristine PEDOT: PSS and d) doped AgNWs@PEDOT: PSS. e) 1D q_z profile extracted from the 2D raw detector mode in q -space, with the PSS halo and PEDOT π - π stacking at $q_z = 1.23$ and $q_z = 1.79$, respectively. AgNWs@PEDOT: PSS was observed at the same q_z for PSS and PEDOT with higher scattering intensity. f) EIS analysis of AgNWs@PEDOT: PSS with the inset of equivalent circuit R_s (R_{ct} //CPE) and the modulus of impedance Z (black curve) and phase angle (orange curve) are plotted as a function of frequency. (For interpretation of the references to colour in this figure legend, the reader is referred to the Web version of this article.)

the electrical double layer effect (EDL, Fig. 1d). The biochemical interaction of the target with the gate would trigger EDL modulation, resulting in the changes of drain-source current. The AgNWs have been regarded as effective dopant to enhance the electronic mobility, however, the doping of PEDOT: PSS by AgNWs to modulate the mobility thus enhance the synergistic determination of biomarkers has not been explored. We compared the performance of pristine PEDOT: PSS and doped AgNWs@PEDOT: PSS (Fig. 2a) as the semiconductor composites of SiOECTs and found that the doping of AgNWs (Fig. S6, Supporting Information) enhanced the drain-source current and corresponding transconductance by 23.1% and 42.3% (Fig. 2a), respectively. We also optimized the ratio of AgNWs/PEDOT: PSS (Fig. S6, Supporting Information) and found the doping of 3.0% AgNWs afforded the optimal outcome of transconductance. As depicted in Fig. S6, there is a dynamic balance between the I_{ds} and g_m as the increase of AgNWs ratio. Specifically, the I_{ds} and g_m for 4.0% AgNWs doping were 265.2 μ A and 0.493 mS in Fig. S6e. The I_{ds} and g_m for 6.0% AgNWs doping were 273.4 μ A and 0.412 mS in Fig. S6f. However, the highest g_m was 0.738 mS at 3.0% AgNWs in Fig. S6d. Notably, we performed statistical analysis of normalized mobility in Fig. 2b and found the normalized mobility of AgNWs@PEDOT: PSS was enhanced from 0.52 ± 0.04 to 0.95 ± 0.08 ($n = 5$). Due to the intrinsic doping characteristics, PEDOT: PSS-based OECTs bioelectronics generally operate in depletion mode. Typical output characteristics of SiOECTs with functionalized gate electrode operating in depletion mode was shown in Fig. S7 [28,29]. The drain-source current (I_{DS}) decreased with increasing bias gate voltage (V_G) [30,31].

Grazing-incidence X-ray scattering (GISAXS) has been widely used to

characterize the intermolecular stacking (e.g., π - π) in semiconductor composites, especially PEDOT: PSS [32,33]. We performed 2D GISAXS analysis of pristine PEDOT: PSS and doped AgNWs@PEDOT: PSS in Fig. 2c–d. The 1D q_z profile extracted from the 2D raw detector mode in q -space were demonstrated in Fig. 2e, with the observations of PSS scattering halo and PEDOT halo with π - π stacking at $q_z = 1.23$ and $q_z = 1.79 \text{ \AA}^{-1}$, respectively [34,35]. Specifically, AgNWs@PEDOT: PSS were observed at the same q_z for PSS and PEDOT with higher scattering intensity, which evidenced the doping of AgNWs@PEDOT: PSS. Meanwhile, the electrochemical impedance spectroscopy analysis (EIS, Fig. 2f) revealed the SiOECTs with passable volumetric capacitance ($90.1 \pm 9.1 \text{ F cm}^{-3}$), which was comparable with other transistor biosensors (Table S1).

2.2. Architecture, mechanism, and experimental validation of pretreatment unit

To validate the feasibility of SiOECTs, we customized tailored pretreatment unit to reduce the heterogeneity/viscosity of sputum specimens. Fig. 3a were typical general views of the SiOECTs, with the exploded view of the PBC electronic system and multiplexed biosensors (with the ZIF connector) for the sputum's pretreatment collection and analysis. Fig. 31a demonstrated the architectural layout of the pretreatment unit with detailed dimensions in Fig. S11b–c. As illustrated in Fig. 3b, there are various bio gels in sputum specimens. Huggins equation Eqs. (1) and (2) illustrates the derivation of the viscosity formula under the effect of η_0 [36].

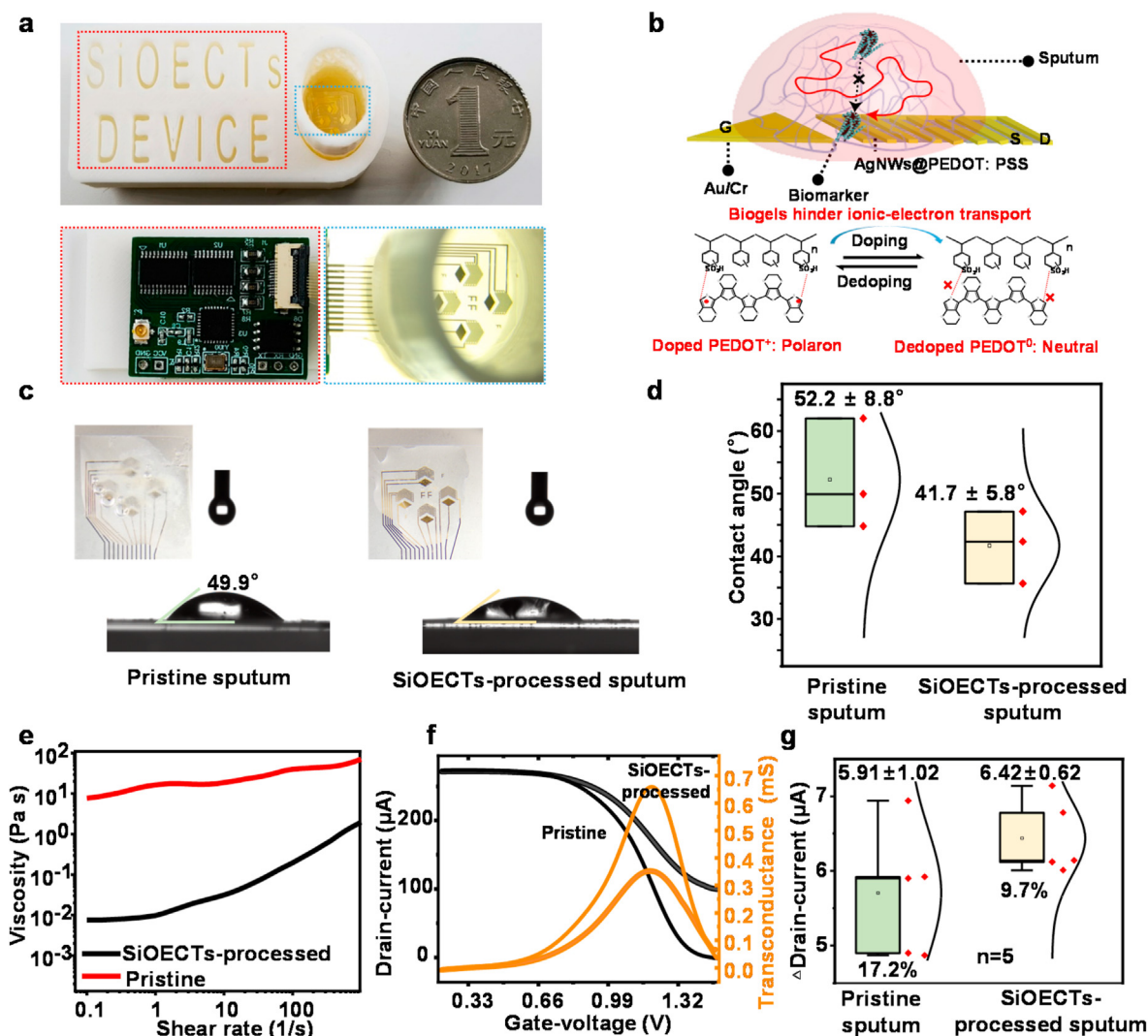


Fig. 3. Mechanism and validations of ion-electron transport recovery in sputum specimens for SiOECTs device. a) Typical photographic images and exploded views of SiOECTs. b) Mechanism of heterogeneity and viscosity for sputum biospecimen. There are various bio gels in sputum specimens, which hinder the ion-electron transfer process. c) Photographic images and contact angles for sputum without/with SiOECTs processing and d) corresponding statistical analysis of contact angles. The contact angles of SiOECTs-pretreated sputum decreased from $52.2 \pm 8.8^\circ$ to $41.7 \pm 5.8^\circ$ due to the integrated design. The standard deviation was calculated by three replicate measurements. e) Viscosity analysis of pristine/SiOECTs-pretreated sputum. The maximum viscosity of SiOECTs-pretreated sputum decreased to 1.95 Pa s by 89.1% under our rheometer configurations. f) Transfer characteristics and corresponding transconductances of sputum without/with SiOECTs processing, resulting in enhanced electron mobility by 88.2% due to the pretreatment unit. g) Statistical analysis of amperometric responses. The SiOECTs-pretreated sputum's amperometric responses ($n = 5$) were enhanced from 5.91 ± 1.02 and 6.42 ± 0.62 μA , and the corresponding coefficient variation (CV) was improved from 17.2% to 9.7%. The standard deviation was calculated by five replicate measurements.

$$\eta_{sp} = \frac{\eta_0 - \eta_s}{\eta_s} \quad (1)$$

η_s is the original viscosity when there are no bio gels in sputum specimens. η_0 is the viscosity of the sputum mixing with an unknown amount of bio gels. The intrinsic viscous property [η] (mL/g) could be analyzed as follows:

$$\eta = \lim_{c \rightarrow 0} \frac{\eta_{sp}}{C} \quad (2)$$

The viscosimeter was used to measure specific viscosities (η_{sp}), and the viscosity formula was adopted to evaluate the viscous property.

Furthermore, the rheological characteristics are influenced by its intrinsic viscosity, contact angle, and surface tension. With a form of the Young equation that accounts for contact angle, the inverse relationship between surface tension and angle is given by: [37]

$$\gamma_{SG} = \gamma_{SL} + \gamma_{LG} \cos \theta_c \quad (3)$$

Where γ_{SG} is solid-gas surface tension, γ_{SL} is solid-liquid surface tension, γ_{LG} is liquid-gas surface tension, and θ is contact angle. Meanwhile, the surface tension (γ) can be extracted using the following equation: [38,39]

$$\eta = \gamma \tau / L \quad (4)$$

Where L is the diameter of the droplet, τ is the relaxation timescale, η and γ are the viscosity and surface tension, respectively, demonstrating the inverse relationship.

The equations mentioned above revealed the influence of bio gels on the viscosity, contact angle, and the surface tension of sputum, which are the critical factors for the sufficient bio-interactions between the sputum's biomarkers and the biosensors/devices and affect the efficiency of the sputum-analytical platform [40–42].

According to the abovementioned formulas and analysis for the viscosity, contact angle, and surface tension, we performed the characterizations of hydrophilicity/hydrophobicity and rheometer analysis, then

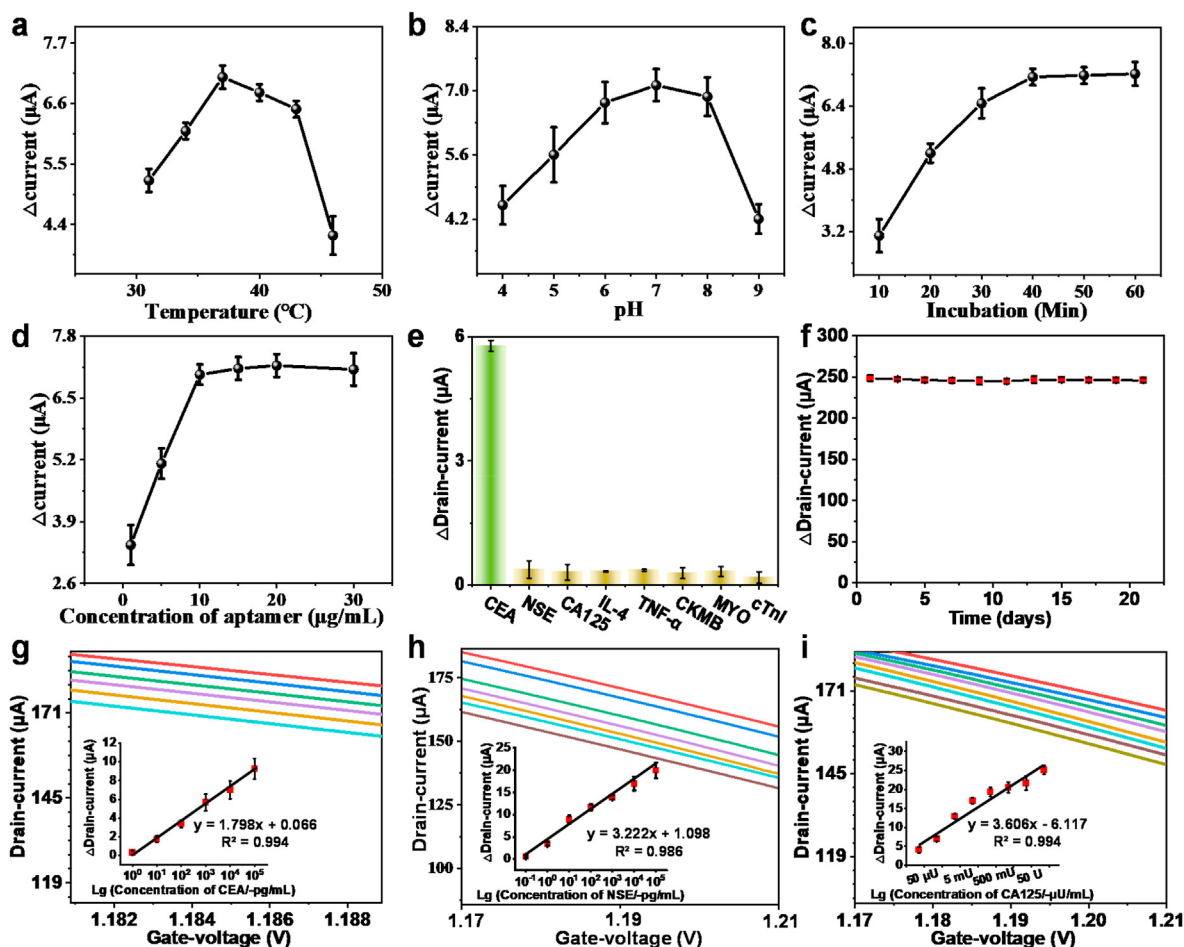


Fig. 4. Optimizations, selectivity, stability, and calibration analysis of SiOECTs. a) Temperatures between 31 and 46 °C was selected, and the temperature of 37.0 °C exhibited an optimal response signal of $7.08 \pm 0.21 \mu\text{A}$. b) pH between 4.0 and 9.0 was optimized with the suitable pH value of 7.0. The best response signal was $7.12 \pm 0.35 \mu\text{A}$. c) Incubation time demonstrated the best performance at 30 min with the value of $7.14 \pm 0.21 \mu\text{A}$. d) 10 $\mu\text{g/mL}$ of aptamer afforded optimized capability with $6.99 \pm 0.21 \mu\text{A}$. e) Selectivity of SiOECTs in the sensing of 1 ng/mL CEA against 10 ng/mL NSE, IL-4, TNF- α , CKMB, MYO, cTnI, and 50 mU/mL CA125. Higher response signals for target biomarkers were observed than those obtained from the interferences. f) Stability of SiOECTs for continuous monitoring within 3 weeks. Typical g) CEA, h) NSE, and i) CA125 calibration curves of SiOECTs with the regression analysis ($n = 3$), and the corresponding inserted plots are the calibration curves of SiOECTs. Error bars in (a–i) represented the standard deviation of three replicate measurements ($n = 3$).

analyzed the influences of hydrophobicity and viscosity on SiOECTs device's performance. It was demonstrated that enhanced amperometric signal and ameliorated coefficient variation validate the pretreatment unit's functionality and shed light on the design on the advanced sputum-analytical platform. Considering the hydrophobic property of sputum for interacting with multiplexed biosensors, the contact angles of sputum decreased from $52.2 \pm 8.8^\circ$ to $41.7 \pm 5.8^\circ$ ($n = 3$, Fig. 3c–d and Fig. S8, Supporting Information) due to integrated design. As demonstrated in Fig. 3e, compared with pristine sputum sample (Index = 33, Table S3), the SiOECTs-pretreated sputum exhibited decreased a maximum viscosity of 1.95 Pa by 89.1% under our rheometer configurations after the pretreatment unit. Notably, the corresponding transfer characteristics on identical SiOECTs-pretreated sputum demonstrated enhanced transconductance by 88.2% (Fig. 3f). Moreover, we conducted the statistical analysis of amperometric current of identical sputum with the experimentally measured values of 5.91 ± 1.02 and $6.42 \pm 0.62 \mu\text{A}$ (Fig. 3g, $n = 5$) for the pristine and SiOECTs-pretreated sputum, respectively. Meanwhile, the ameliorated coefficient variation (CV) of SiOECTs was improved from 17.2% to 9.7% (Fig. 3g, $n = 5$), which was critical for the advanced sputum-analytical platform. These characterizations verified the functionality of the pretreatment unit, resulting in reduced viscosity/contact angle and ameliorated signals, which laid the foundations for the subsequently accurate quantification of biomarkers.

2.3. Characterizations, performance, and calibrations of SiOECTs

On account of interactions among the aptamer, the sputum biomarker, and the electrolyte, parameters of the SiOECTs device, including temperature, pH, binding time, and aptamer amount, were selectively optimized for comparisons (Fig. 4a–d). The optimal parameters of the temperature (37.0 °C, Fig. 4a) and pH value (7.0, Fig. 4b) indicated the suitable configurations for SiOECTs. We tested the pH of 12 clinical sputum samples (shown in Fig. S9) and found the average pH value of 7.2 ± 0.1 . The pH value of actual sputum biosamples is close to the test parameters for the SiOECTs device. Incubation time demonstrated the best performance at 30 min with the value of $7.14 \pm 0.21 \mu\text{A}$ (Fig. 4c) and 10 $\mu\text{g/mL}$ of aptamer afforded optimized capability with $6.99 \pm 0.21 \mu\text{A}$ (Fig. 4d).

Amperometric measurements were performed by adding various interfering molecules to illuminate the selectivity of the SiOECTs device for a panel of biomarkers. As for interfering molecules, specific protein biomarkers including CEA, NSE, CA125, IL-4, TNF- α , CKMB, MYO, and cTnI were selected. For the specificity evaluation, we selected changed current ($\Delta\text{current}$) for comparisons in the biosensing of CEA. As demonstrated in Fig. 4e, The SiOECTs displayed a notable current change ($\Delta\text{current} = 5.78 \pm 0.13 \mu\text{A}$) in the biosensing of 1 ng/mL CEA. In contrast, we observed relatively low responses in the quantification of 10

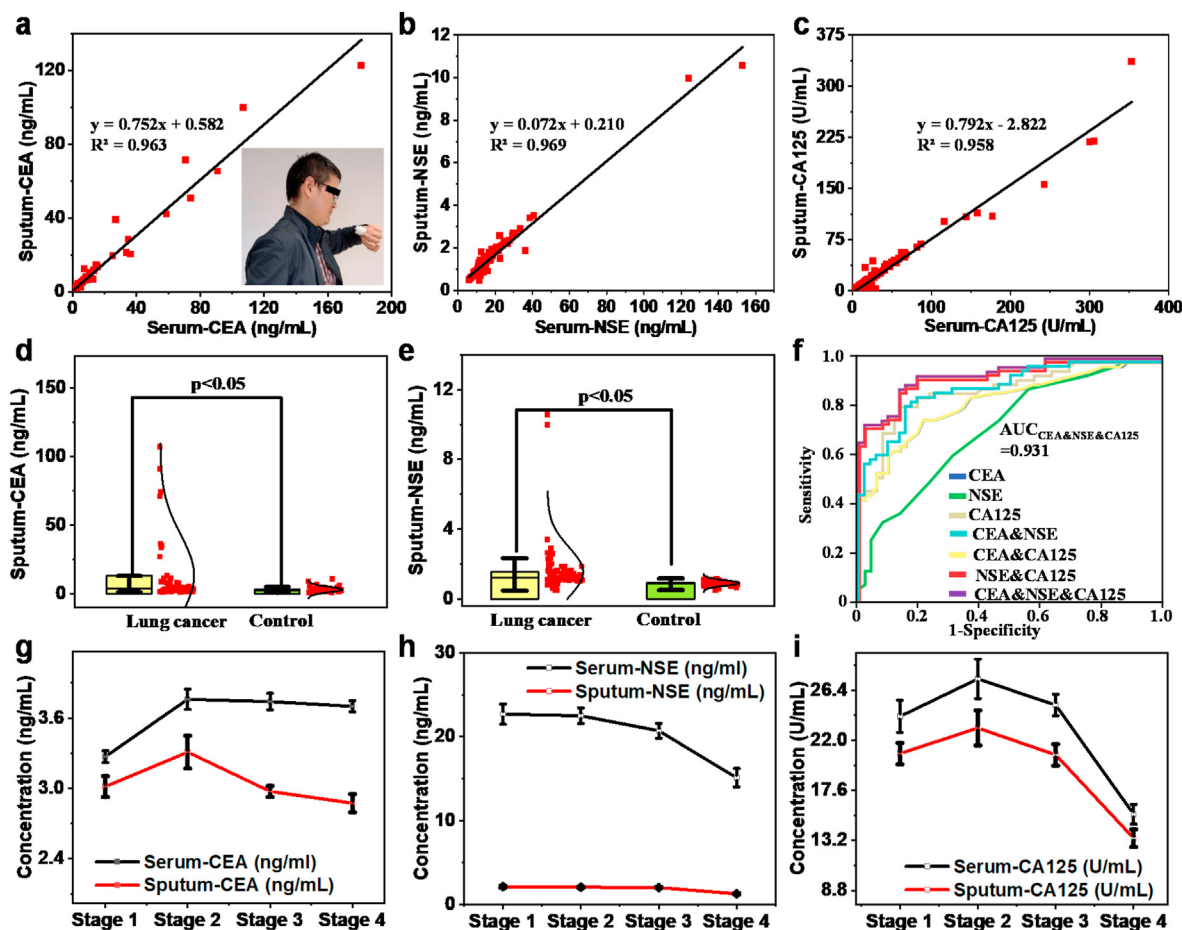


Fig. 5. Diagnosis/monitoring of lung cancer and its clinic's performance. a) CEA, b) NSE, and c) CA125 correlation relationship between serum and pretreated sputum among 106 clinical cohorts with favorable correction coefficient of 0.963, 0.969, and 0.958, respectively. The inset is the photograph of SiOECTs assembled around the wrist. Users can conveniently operate SiOECTs devices rather than rely on professionally trained people. Student's t-testing for significance evaluation between lung cancer ($n = 54$) and healthy control ($n = 52$) for d) CEA and e) NSE with $p < 0.05$. f) Receiver operating curve analysis of single biomarker and combined biomarkers towards 106 clinical raw sputum biospecimens (52 healthy controls vs 54 lung cancer patients). g) CEA, h) NSE, and i) CA125 monitoring of one subject (lung cancer) after chemotherapy/radiotherapy over 16-weeks periods. The CEA and CA125 demonstrated the trend of first rising and then falling. The NSE exhibited a continuous falling trend. The monitoring capability of SiOECTs would assist guidance of radiotherapy/chemotherapy for lung cancer. Error bars in (g–i) represented the standard deviation of three replicate measurements ($n = 3$).

ng/mL NSE ($0.38 \pm 0.21 \mu\text{A}$), 50 mU/mL CA125 ($0.31 \pm 0.19 \mu\text{A}$), 10 ng/mL IL-4 ($0.33 \pm 0.16 \mu\text{A}$), 10 ng/mL TNF- α ($0.36 \pm 0.24 \mu\text{A}$), 10 ng/mL CKMB ($0.29 \pm 0.13 \mu\text{A}$), 10 ng/mL MYO ($0.33 \pm 0.12 \mu\text{A}$) and 10 ng/mL cTnI ($0.18 \pm 0.14 \mu\text{A}$). The favorable selectivity could be attributed to the high affinity of the aptamer with optimized parameters, hindering nonspecific binding. The selectivity characterizations of NSE and CA125 were demonstrated in Fig. S10, resulting in much higher response signals for target biomarkers than obtained from the interferences (IL-4, TNF- α , CKMB, MYO, and cTnI), which as a whole indicated the specific sensing of panel biomarkers. We also tested the stability of the SiOECTs by recording the amperometric current. The device exhibited high stability lasted for three weeks (Fig. 4f). As shown in Fig. 4g, the proposed SiOECTs afforded sensitive quantification of CEA with ultra-wide linear ranges 1.0 pg/mL– 1.0×10^5 pg/mL (correlation coefficient R^2 value of 0.994). For the calibration of NSE and CA125, the SiOECTs also presented wide linear ranges and favorable correlation coefficients as displayed in Fig. 4h–i, which were comparable with other blood-type biosensors (Table S2, Supporting Information).

2.4. Clinical sputum assay with SiOECTs

Due to the merits of intrinsic amplification effect, quick response, high signal-noise ratio, and accessible integration, our SiOECTs device

potentially could be an advanced sputum-analytical platform for non-invasive clinic POCT. Herein, our wrist-portable device was applied to detect biomarkers of raw sputum biospecimens from clinic lung cancer patients in a non-invasive manner. We utilized SiOECTs to test raw sputum specimen from 52 healthy controls and 54 lung cancer patients to evaluate its diagnosis performance and optimize its panel biomarkers (Table S3-4). As demonstrated in Fig. 5a, the CEA calibration curve afforded a correction coefficient of $R^2 = 0.963$, with the linear relationship of $\text{Concentration}_{\text{sputum-CEA}} = 0.752 \times \text{Concentration}_{\text{serum-CEA}} + 0.582$. The concentrations of biomarkers (e.g., CEA, NSE) in serum were measured by electrochemiluminescence assay (COBAS e801, Roche). Meanwhile, we compared clinical trials for NSE and CA125 with a high correlation coefficient of 0.969 and 0.958, respectively, as depicted in Fig. 5b–c. Moreover, significant differences in CEA and NSE were observed between the 52 healthy controls and 54 lung cancer patients with p -value < 0.05 (Fig. 5d–e, Student's t-test, Table S3).

Moreover, a single biomarker is insufficient to diagnose lung cancer in terms of specificity and selectivity. The multiplexed biosensor is an efficient strategy for simultaneous detection towards accurate diagnostics [43,44]. We utilized the multi-channels design of organic electrochemical transistors to address the subsequent signal recording while maintaining its miniaturization. The area under the curve (AUC) was used to evaluate the diagnostic performance of biomarkers, and AUC

higher than 0.9 indicates favorable diagnostic efficacy [45,46]. As displayed in Fig. 5f, any individual biomarker (e.g., CEA, NSE, and CA125) failed to harvest satisfying AUC with 0.837, 0.727, and 0.884 for CEA, NSE, and CA125, respectively (Table S4). In the dual biomarkers analysis, the analysis yielded the enhanced AUC value of 0.838, 0.924, and 0.891 for the combination of CEA&NSE, CEA&CA125, and NSE&CA125, respectively (Table S4). Finally, the optimum diagnosis performance was achieved via triple biomarkers combination with an AUC value of 0.931, while the sensitivity value is 87.0%, and the specificity value is 86.5%. (Table S4). Notably, the diagnosis capability was improved with the merit of multiplexed biosensors assembled on a molecularly tailored SiOECTs device. Practical clinical trials proved that our device is applicable to detect sputum samples, accurately assisting clinical disease diagnosis.

Furthermore, convenient operation and miniaturization are the necessary considerations for the universal deployment of the portable biosensor in clinics. Our fully integrated SiOECTs device could be comfortably and conveniently assembled around the wrist (inset in Fig. 5a), which is advantageous for lung cancer patient's in-home diagnosis and health monitoring. Herein, we realized the continuous tracking for the changes of typical biomarkers in lung cancer patients' sputum. Specifically, the values of biomarkers in sputum and serum were observed toward monitoring three lung cancer patients after chemotherapy/radiotherapy over 16 weeks (Fig. 5g–i, Fig. S11, Table S3, Supporting Information). Both in sputum (by our device) and serum (by electrochemiluminescence assay, COBAS e801, Roche) biospecimens, the CEA (Fig. 5g) and CA125 (Fig. 5i) demonstrated the trend of first rising and then falling. At the same time, the NSE (Fig. 5h) exhibited a continuous falling trend. As depicted in Fig. S12, statistical analysis of sputum biospecimens demonstrated a favorable correlation coefficient between the serum and sputum values for CEA, NSE, and CA125. Moreover, due to the miniaturization design of our wrist-portable SiOECTs, patients can conveniently operate SiOECTs devices by themselves rather than rely on professionally trained people (Fig. S13, Supporting Information). Our SiOECTs devices would enable continuous in-home detection and monitoring for the health surveillance of lung cancer patients after radiotherapy/chemotherapy.

3. Conclusions

This work introduced a miniaturized and wrist-portable bioelectronic device based on sputum biospecimens diagnosis. We utilized the molecularly tailored multiplexed AgNWs-doped interdigitated organic electrochemical transistors as the biosensors. In the device design, the doping of PEDOT: PSS by AgNWs was utilized to recover and increase mobility, thus enhancing the synergistic quantification of biomarkers. Notably, the integrated device enables the recovery of ionic-electron transport in sputum specimens, thus drastically enhanced electron mobility. This device is capable for noninvasive and continuous clinic diagnosis/monitoring of lung cancer via multiplexed biosensing. Furthermore, with multiplexed biosensing design, our SiOECTs could achieve the detection of CEA, NSE, and CA125 in human sputum biospecimens simultaneously. Particularly, by the multi-channel analysis of triple biomarkers, our device can achieve optimum diagnosis capability of lung cancer patients against healthy individuals with an AUC of 0.931, a sensitivity of 87.0%, and a specificity of 86.5%. Moreover, due to the merits of quick response, high signal-noise ratio, miniaturization, and wrist-portability, patients could conveniently self-operate the wrist-portable SiOECTs device for health monitoring without specialized training. Abovementioned merits collectively demonstrated the practical deployment of SiOECTs and could pave an avenue for noninvasive health surveillance of sputum-related diseases in the clinics.

CRedit author statement

Ru Zhang: Investigation, Original draft preparation. **Jing Zhang:**

Investigation. **Fei Tan:** Reviewing. **Deqi Yang:** Software. **Bingfang Wang:** Validation. **Jing Dai:** Software. **Yin Qi:** Characterizations. **Linyu Ran:** Characterizations. **Wenjuan He:** Characterizations. **Yingying Lv:** Reviewing. **Feilong Wang:** Supervision. **Yin Fang:** Supervision, Writing-Reviewing and Editing.

Declaration of competing interest

The authors declare that they have no known competing financial interests or personal relationships that could have appeared to influence the work reported in this paper.

Acknowledgements

This project was supported by National Key Research and Development Program (2022YFE0100400), National Natural Science Foundation of China (82001960), Science and Technology Commission of Shanghai Municipality (21ZR1465200), Shanghai Municipal Science and Technology Major Project (2021SHZDX0100), the Fundamental Research Funds for the Central Universities, China Postdoctoral Science Foundation (2020M681395), Super Postdoc Project of Shanghai City (2020431). R.Z. and J. Z. contributed equally to this work.

Appendix A. Supplementary data

Supplementary data to this article can be found online at <https://doi.org/10.1016/j.mtbio.2022.100385>.

References

- [1] O. Parlak, S.T. Keene, A. Marais, V.F. Curto, A. Salleo, Molecularly selective nanoporous membrane-based wearable organic electrochemical device for noninvasive cortisol sensing, *Sci. Adv.* 4 (2018) aar2904, <https://doi.org/10.1126/sciadv.aar2904>.
- [2] J. Cheong, H. Yu, C.Y. Lee, J. uk Lee, H.J. Choi, J.H. Lee, H. Lee, J. Cheon, Fast detection of SARS-CoV-2 RNA via the integration of plasmonic thermocycling and fluorescence detection in a portable device, *Nat. Biomed. Eng.* 4 (2020) 1159–1167, <https://doi.org/10.1038/s41551-020-00654-0>.
- [3] G.H. Lee, H. Moon, H. Kim, G.H. Lee, W. Kwon, S. Yoo, D. Myung, S.H. Yun, Z. Bao, S.K. Hahn, Multifunctional materials for implantable and wearable photonic healthcare devices, *Nat. Rev. Mater.* 5 (2020) 149–165, <https://doi.org/10.1038/s41578-019-0167-3>.
- [4] A.J. Bandodkar, P. Gutruf, J. Choi, K.H. Lee, Y. Sekine, J.T. Reeder, W.J. Jeang, A.J. Aranyosi, S.P. Lee, J.B. Model, R. Ghaffari, C.J. Su, J.P. Leshock, T. Ray, A. Verrillo, K. Thomas, V. Krishnamurthi, S. Han, J. Kim, S. Krishnan, T. Hang, J.A. Rogers, Battery-free, skin-interfaced microfluidic/electronic systems for simultaneous electrochemical, colorimetric, and volumetric analysis of sweat, *Sci. Adv.* 5 (2019) aav3294, <https://doi.org/10.1126/sciadv.aav3294>.
- [5] J. Kim, J.R. Sempionatto, S. Imani, M.C. Hartel, A. Barfidokht, G. Tang, A.S. Campbell, P.P. Mercier, J. Wang, Simultaneous monitoring of sweat and interstitial fluid using a single wearable biosensor platform, *Adv. Sci.* 5 (2018), 201800880, <https://doi.org/10.1002/adv.201800880>.
- [6] M. Bariya, H.Y.Y. Nyein, A. Javey, Wearable sweat sensors, *Nat. Electron.* 1 (2018) 160–171, <https://doi.org/10.1038/s41928-018-0043-y>.
- [7] M. Trzaskowski, A. Napiórkowska, E. Augustynowicz-Kopec, T. Ciach, Detection of tuberculosis in patients with the use of portable SPR device, *Sensor. Actuator. B Chem.* 260 (2018) 786–792, <https://doi.org/10.1016/j.snb.2017.12.183>.
- [8] B.A. Prabowo, Y.F. Chang, H.C. Lai, A. Alom, P. Pal, Y.Y. Lee, N.F. Chiu, K. Hatanaka, L.C. Su, K.C. Liu, Rapid screening of Mycobacterium tuberculosis complex (MTBC) in clinical samples by a modular portable biosensor, *Sensor. Actuator. B Chem.* 254 (2018) 742–748, <https://doi.org/10.1016/j.snb.2017.07.102>.
- [9] Z.S. Miripour, R. Sarrami-Forooshani, H. Sanati, J. Makarem, M.S. Taheri, F. Shojaeian, A.H. Eskafi, F. Abbasvandi, N. Namdar, H. Ghafari, P. Aghaee, A. Zandi, M. Faramarzpour, M. Hoseinyazdi, M. Tayebi, M. Abdolabad, Real-time diagnosis of reactive oxygen species (ROS) in fresh sputum by electrochemical tracing; correlation between COVID-19 and viral-induced ROS in lung/respiratory epithelium during this pandemic, *Biosens. Bioelectron.* 165 (2020), <https://doi.org/10.1016/j.bios.2020.112435>.
- [10] Y. Chen, S. Guo, M. Zhao, P. Zhang, Z. Xin, J. Tao, L. Bai, Amperometric DNA biosensor for Mycobacterium tuberculosis detection using flower-like carbon nanotubes-polyaniline nanohybrid and enzyme-assisted signal amplification strategy, *Biosens. Bioelectron.* 119 (2018) 215–220, <https://doi.org/10.1016/j.bios.2018.08.023>.
- [11] F. Massai, F. Imperi, S. Quattrucci, E. Zennaro, P. Visca, L. Leoni, A multitask biosensor for micro-volumetric detection of N-3-oxo-dodecanoyl-homoserine

- lactone quorum sensing signal, *Biosens. Bioelectron.* 26 (2011) 3444–3449, <https://doi.org/10.1016/j.bios.2011.01.022>.
- [12] J. Schneider, Early detection of lung cancers - comparison of computed tomography, cytology and fuzzy-based tumor markers panels, *Cancer Biomarkers* 6 (2010) 149–162, <https://doi.org/10.3233/CBM-2009-0126>.
- [13] W. Wu, S. Bang, E.R. Bleecker, M. Castro, L. Denlinger, S.C. Erzurum, J. V. Fahy, A.M. Fitzpatrick, B.M. Gaston, A.T. Hastie, E. Israel, N.N. Jarjour, B.D. Levy, D.T. Mauger, D.A. Meyers, W.C. Moore, M. Peters, B.R. Phillips, W. Phipatanakul, R.L. Sorkness, S.E. Wenzel, Multiview cluster Analysis identifies variable corticosteroid response phenotypes in severe asthma, *Am. J. Respir. Crit. Care Med.* 199 (2019) 1358–1367, <https://doi.org/10.1164/rccm.201808-1543OC>.
- [14] S. Datta, L. Shah, R.H. Gilman, C.A. Evans, Comparison of sputum collection methods for tuberculosis diagnosis: a systematic review and pairwise and network meta-analysis, *Lancet Global Health* 5 (2017), [https://doi.org/10.1016/S2214-109X\(17\)30201-2](https://doi.org/10.1016/S2214-109X(17)30201-2) e760–e771.
- [15] J. Leal, X. Peng, X. Liu, D. Arasappan, D.C. Wylie, S.H. Schwartz, J.J. Fullmer, B.C. McWilliams, H.D.C. Smyth, D. Ghosh, Peptides as surface coatings of nanoparticles that penetrate human cystic fibrosis sputum and uniformly distribute in vivo following pulmonary delivery, *J. Contr. Release* 322 (2020) 457–469, <https://doi.org/10.1016/j.jconrel.2020.03.032>.
- [16] S.C. Kerr, S.D. Carrington, S. Yuan, M. Solon, J.V. Fahy, Galactose binding lectins cross-link airway mucins and are a novel mediator of mucus plug formation in acute asthma, *Am. Thorac. Soc.* (2010), https://doi.org/10.1164/ajrccm-conference.2010.181.1_meetingabstracts.a5510. A5510–A5510.
- [17] C. Cea, G.D. Spyropoulos, P. Jastrzebska-Perfect, J.J. Ferrero, J.N. Gelinias, D. Khodagholi, Enhancement-mode ion-based transistor as a comprehensive interface and real-time processing unit for in vivo electrophysiology, *Nat. Mater.* 19 (2020) 679–686, <https://doi.org/10.1038/s41563-020-0638-3>.
- [18] G. Méhes, A. Roy, X. Strakosas, M. Berggren, E. Stavrinidou, D.T. Simon, Organic microbial electrochemical transistor monitoring extracellular electron transfer, *Adv. Sci.* 7 (2020), 2000641, <https://doi.org/10.1002/advs.202000641>.
- [19] X. Guo, Q. Cao, Y. Liu, T. He, J. Liu, S. Huang, H. Tang, M. Ma, Organic electrochemical transistor for in situ detection of H₂O₂ released from adherent cells and its application in evaluating the in vitro cytotoxicity of nanomaterial, *Anal. Chem.* 92 (2020) 908–915, <https://doi.org/10.1021/acs.analchem.9b03718.s001>.
- [20] H. Liu, A. Yang, J. Song, N. Wang, P. Lam, Y. Li, H.K.-W. Law, F. Yan, Ultrafast, sensitive, and portable detection of COVID-19 IgG using flexible organic electrochemical transistors, *Sci. Adv.* 7 (2021), eabg8387, <https://doi.org/10.1126/sciadv.abg8387>.
- [21] W. Lee, D. Kim, N. Matsuhisa, M. Nagase, M. Sekino, G.G. Malliaras, T. Yokota, T. Someya, Transparent, conformable, active multielectrode array using organic electrochemical transistors, *Proc. Natl. Acad. Sci. U.S.A.* 114 (2017) 10554–10559, <https://doi.org/10.1073/pnas.1703886114>.
- [22] A. Yang, Y. Li, C. Yang, Y. Fu, N. Wang, L. Li, F. Yan, Fabric organic electrochemical transistors for biosensors, *Adv. Mater.* 30 (2018) 1–8, <https://doi.org/10.1002/adma.201800051>.
- [23] X. Zhang, B. Wang, L. Huang, W. Huang, Z. Wang, W. Zhu, Y. Chen, Y.L. Mao, A. Facchetti, T.J. Marks, Breath figure-derived porous semiconducting films for organic electronics, *Sci. Adv.* 6 (2020) 1–10, <https://doi.org/10.1126/sciadv.aaz1042>.
- [24] P. Xie, T. Liu, J. Sun, J. Jiang, Y. Yuan, Y. Gao, J. Zhou, J. Yang, Solution-processed ultra-flexible C8-BTBT organic thin-film transistors with the corrected mobility over 18 cm²/(V s), *Sci. Bull.* 65 (2020) 791–795, <https://doi.org/10.1016/j.scib.2020.03.013>.
- [25] X. Ji, H.Y. Lau, X. Ren, B. Peng, P. Zhai, S.P. Feng, P.K.L. Chan, Highly sensitive metabolite biosensor based on organic electrochemical transistor integrated with microfluidic channel and poly(N-vinyl-2-pyrrolidone)-Capped platinum nanoparticles, *Adv. Mater. Technol.* 1 (2016), <https://doi.org/10.1002/admt.201600042>.
- [26] C.G. Bischak, L.Q. Flagg, D.S. Ginger, Ion exchange gels allow organic electrochemical transistor operation with hydrophobic polymers in aqueous solution, *Adv. Mater.* 32 (2020), <https://doi.org/10.1002/adma.202002610>.
- [27] S. Inal, J. Rivnay, A.O. Suiu, G.G. Malliaras, I. McCulloch, Conjugated polymers in bioelectronics, *Acc. Chem. Res.* 51 (2018) 1368–1376, <https://doi.org/10.1021/acs.accounts.7b00624>.
- [28] S.T. Keene, T.P.A. van der Pol, D. Zakhidov, C.H.L. Weijtens, R.A.J. Janssen, A. Salleo, Y. van de Burgt, Enhancement-mode PEDOT:PSS organic electrochemical transistors using molecular de-doping, *Adv. Mater.* 32 (2020), <https://doi.org/10.1002/adma.202000270>.
- [29] G. Gaál, M.L. Braunger, V. Rodrigues, A. Riul, H.L. Gomes, High electrical anisotropic multilayered self-assembled organic films based on graphene oxide and PEDOT:PSS, *Adv. Electron. Mater.* 7 (2021), <https://doi.org/10.1002/aelm.202100255>.
- [30] V. Venkatraman, J.T. Friedlein, A. Giovannitti, I.P. Maria, I. McCulloch, R.R. McLeod, J. Rivnay, Subthreshold operation of organic electrochemical transistors for biosignal amplification, *Adv. Sci.* 5 (2018) 1–7, <https://doi.org/10.1002/advs.201800453>.
- [31] N. Saraf, E.R. Woods, M. Pepler, S. Seal, Highly selective aptamer based organic electrochemical biosensor with pico-level detection, *Biosens. Bioelectron.* 117 (2018) 40–46, <https://doi.org/10.1016/j.bios.2018.05.031>.
- [32] A. Savva, R. Hallani, C. Cendra, J. Surgailis, T.C. Hidalgo, S. Wustoni, R. Sheelamantula, X. Chen, M. Kirkus, A. Giovannitti, A. Salleo, I. McCulloch, S. Inal, Balancing ionic and electronic conduction for high-performance organic electrochemical transistors, *Adv. Funct. Mater.* 30 (2020) 1–9, <https://doi.org/10.1002/adfm.201907657>.
- [33] C.G. Bischak, L.Q. Flagg, K. Yan, C.Z. Li, D.S. Ginger, Fullerene active layers for n-type organic electrochemical transistors, *ACS Appl. Mater. Interfaces* 11 (2019) 28138–28144, <https://doi.org/10.1021/acsami.9b11370>.
- [34] X. Wu, A. Surendran, J. Ko, O. Filoniik, E.M. Herzog, P. Müller-Buschbaum, W.L. Leong, Ionic-liquid doping enables high transconductance, fast response time, and high ion sensitivity in organic electrochemical transistors, *Adv. Mater.* 31 (2019) 1–9, <https://doi.org/10.1002/adma.201805544>.
- [35] S.M. Kim, C.H. Kim, Y. Kim, N. Kim, W.J. Lee, E.H. Lee, D. Kim, S. Park, K. Lee, J. Rivnay, M.H. Yoon, Influence of PEDOT:PSS crystallinity and composition on electrochemical transistor performance and long-term stability, *Nat. Commun.* 9 (2018), <https://doi.org/10.1038/s41467-018-06084-6>.
- [36] S. Gillet, M. Aguedo, R. Petrut, G. Olive, P. Anastas, C. Blecker, A. Richel, Structure impact of two galactomannan fractions on their viscosity properties in dilute solution, unperturbed state and gel state, *Int. J. Biol. Macromol.* 96 (2017) 550–559, <https://doi.org/10.1016/j.ijbiomac.2016.12.057>.
- [37] T. Huhtamäki, X. Tian, J.T. Korhonen, R.H.A. Ras, Surface-wetting characterization using contact-angle measurements, *Nat. Protoc.* 13 (2018) 1521–1538, <https://doi.org/10.1038/s41596-018-0003-z>.
- [38] I. Alshareedah, T. Kaur, P.R. Banerjee, Methods for characterizing the material properties of biomolecular condensates, *Methods Enzymol.* 646 (2021) 143–183, <https://doi.org/10.1016/bs.mie.2020.06.009>.
- [39] I. Alshareedah, G.M. Thurston, P.R. Banerjee, Quantifying viscosity and surface tension of multicomponent protein-nucleic acid condensates, *Biophys. J.* 120 (2021) 1161–1169, <https://doi.org/10.1016/j.bpj.2021.01.005>.
- [40] S. Kloß, B. Lorenz, S. Dees, I. Labugger, P. Rösch, J. Popp, Destruction-free procedure for the isolation of bacteria from sputum samples for Raman spectroscopic analysis, *Anal. Bioanal. Chem.* 407 (2015) 8333–8341, <https://doi.org/10.1007/s00216-015-8743-x>.
- [41] R. Tyagi, C. Witte, R. Haag, L. Schröder, Dendronized cryptophanes as water-soluble xenon hosts for (129)Xe magnetic resonance imaging, *Org. Lett.* 16 (2014) 4436–4439, <https://doi.org/10.1021/ol501951z>.
- [42] V.A.T. Nguyen, H. Van Nguyen, T. Van Dinh, H.H. Du, C.N. Do, G.B. Marks, N.V. Nguyen, Evaluation of LoopampTM MTBC detection kit for diagnosis of pulmonary tuberculosis at a peripheral laboratory in a high burden setting, *Diagn. Microbiol. Infect. Dis.* 90 (2018) 190–195, <https://doi.org/10.1016/j.diagmicrobio.2017.11.009>.
- [43] I. Kalomenidis, K. Dimakou, A. Kolintza, K. Vlami, M. Papadakis, C. Sotiropoulou, D. Orphanidou, C. Roussos, S. Papiiris, Sputum carcinoembryonic antigen, neuron-specific enolase and cytokeratin fragment 19 levels in lung cancer diagnosis, *Respirology* 9 (2004) 54–59, <https://doi.org/10.1111/j.1440-1843.2003.00536.x>.
- [44] B. Liu, Y. Li, H. Wan, L. Wang, W. Xu, S. Zhu, Y. Liang, B. Zhang, J. Lou, H. Dai, K. Qian, High performance, multiplexed lung cancer biomarker detection on a plasmonic gold chip, *Adv. Funct. Mater.* 26 (2016) 7994–8002, <https://doi.org/10.1002/adfm.201603547>.
- [45] J. McKiernan, M.J. Donovan, V. O'Neill, S. Bentink, M. Noerholm, S. Belzer, J. Skog, M.W. Kattan, A. Partin, G. Andriole, G. Brown, J.T. Wei, I.M. Thompson, P. Carroll, A novel urine exosome gene expression assay to predict high-grade prostate cancer at initial biopsy, *JAMA Oncol.* 2 (2016) 882–889, <https://doi.org/10.1001/jamaoncol.2016.0097>.
- [46] L. Huang, J. Wan, X. Wei, Y. Liu, J. Huang, X. Sun, R. Zhang, D.D. Gurav, V. Vedarethinam, Y. Li, R. Chen, K. Qian, Plasmonic silver nanoshells for drug and metabolite detection, *Nat. Commun.* 8 (2017) 220, <https://doi.org/10.1038/s41467-017-00220-4>.